Research Article

GPR101 loss promotes insulin resistance and diet-induced obesity risk

Lillian Garrett [a,b], Martin Irmler [a], Angela Baljuls [j], Birgit Rathkolb [a,g,h], Nathalia Dragano [a], Raffaele Gerlini [a,g], Adrián Sanz-Moreno [a], Antonio Aguilar-Pimentel [a], Lore Becker [a], Markus Kraiger [a], Rosa Reithmeir [b,i], Johannes Beckers [a,f,g], Julia Calzada-Wack [a], Wolfgang Wurst [b,c,d,e], Helmut Fuchs [a], Valerie Gailus-Durner [a], Tina Zimmermann [j,1], Sabine M. Hölter [a,b,i,1,*], Martin Hrabĕ de Angelis [a,f,g,1,**]

[a] Institute of Experimental Genetics and German Mouse Clinic, Helmholtz Zentrum München, German Research Center for Environmental Health, Neuherberg, Germany
[b] Institute of Developmental Genetics, Helmholtz Zentrum München, German Research Center for Environmental Health, Neuherberg, Germany
[c] TUM School of Life Sciences, Technische Universität München, Freising-Weihenstephan, Germany
[d] Deutsches Institut für Neurodegenerative Erkrankungen (DZNE) Site Munich, Feodor-Lynen-Str. 17, 81377, Munich, Germany
[e] Munich Cluster for Systems Neurology (SyNergy), Adolf-Butenandt-Institut, Ludwig-Maximilians-Universität München, Feodor-Lynen-Str. 17, 81377, Munich, Germany
[f] TUM School of Life Sciences, Technische Universität München, Alte Akademie 8, 85354, Freising, Germany
[g] German Center for Diabetes Research (DZD), Ingolstädter Landstr. 1, 85764, Neuherberg, Germany
[h] Institute of Molecular Animal Breeding and Biotechnology, Gene Center, Ludwig-Maximilians University Munich, Munich, Germany
[i] Technische Universität München, Freising-Weihenstephan, Germany
[j] Boehringer Ingelheim Pharma GmbH & Co. KG, Birkendorfer Straße 65, 88397, Biberach an der Riss, Germany

ARTICLE INFO

ABSTRACT

G-protein-coupled receptors (GPCRs) represent targets for improved low-side-effect therapies to tackle the evolving Western obesity epidemic. The orphan (o) GPCR GPR101 emerged as an attractive candidate in this regard. Expressed on cells in brain areas regulating energy homeostasis, including the hunger-suppressing proopiomelanocortin (POMC) + neurons, it is minimally expressed outside the brain. To understand the function of this receptor *in vivo*, we herein generated and comprehensively characterized a *Gpr101* knockout mouse line, either under standard feeding conditions or with chronic high-fat diet (HFD) access (16 weeks). GPR101 loss accelerated the risk for diet-induced obesity (DIO), hyperinsulinemia and disrupted glucose homeostasis. Hypothalamic transcriptomic analysis revealed also decreased *Pomc* activation with HFD suggesting impaired hunger suppression. Moreover, on a standard diet, there was a molecular signature of downregulated tristetraprolin (TTP) interactome gene activation suggesting impaired inflammation resolution. On HFD, there was differential expression of genes involved in microglial phagocytosis and lipid metabolism. Morphometry revealed altered hypothalamic arcuate nucleus microglial morphology consistent with the transcriptomic profile. We discuss how the GPR101 specialized pro-resolving mediator (SPM) receptor capacity likely underlies the aberrant microglial function and contributes to DIO risk. Thus, this evidence shows that GPR101 is a potential therapeutic target for DIO through, among other factors, effects on hypothalamic inflammation resolution.

1. Introduction

According to the World Health Organisation (WHO), obesity prevalence numbers in Western society have almost tripled in the last 40 years. This is paralleled by increases in obesity-associated metabolic disorders including Type II diabetes (T2D), cardiovascular disease and non-alcoholic fatty liver disease (NAFLD) further impacting patient life quality and increasing mortality rates (Gregg et al., 2019; Saeedi et al., 2019). In certain cases, successful weight reduction and T2D treatment necessitate pharmacological intervention and so there is the need to develop more safe and efficacious therapies. In this regard, 'orphan' G-protein coupled receptors (oGPCRs), part of the seven

transmembrane-spanning domain receptor family, localized to brain areas controlling feeding and energy balance regulation, provide novel and attractive therapeutic targets. While there is progress in GPCR deorphanization, the ongoing challenge lies in establishing the endogenous ligand(s) and function of these orphan receptors to determine their likely efficacy and potential side-effect profile (Ngo et al., 2016).

The class A oGPCR, GPR101, is of interest in this context. This receptor couples to G_s, $G_{q/11}$, and $G_{12/13}$ and strongly activates cAMP (Abboud et al., 2020). It is highly expressed in the brain, specifically in regions that control metabolism, reward and emotionality including the amygdala, nucleus accumbens and the arcuate nucleus (ARC) of the hypothalamus (Bates et al., 2006; Lee et al., 2001; Trivellin et al., 2016). Within these regions, GPR101 is expressed in ~55% of the anorexigenic proopiomelanocortin (POMC)+ neurons in ARC, glutamatergic neurons and thyrotropin-releasing hormone (TRH)+ neurons in the lateral hypothalamus and in a subset of γ-aminobutyric acid (GABA)+ and dopaminergic neurons in the ventral tegmental area (VTA) and substantia nigra (SN) (Nilaweera et al., 2007; Paul et al., 2019). While the physiology, function and known ligands of GPR101 remain largely unexplored, expression in different brain regions alters after energetic challenges e.g. food deprivation and during lactation (Nilaweera et al. 2007, 2008). This suggests an important role for GPR101 in energy homeostasis, a possibility supported by evidence of a SNP in the *GPR101* coding sequence associated with increased BMI in the Japanese population (missense variant (rs1190736 (C > A); p.Val124Leu)) (Akiyama et al., 2017). The developing pituitary gland also expresses GPR101. In humans, a pediatric disorder, X-linked acrogigantism (X-LAG), results from an Xq26.3 genomic duplication involving *GPR101,* characterized by early-onset gigantism due to hypersecretion of growth hormone (GH) (Trivellin et al., 2014). Moreover, in mice, overexpression of *Gpr101* under the control of the rat *Ghrhr* (growth hormone releasing hormone receptor) promoter (expressed in anterior pituitary somatotrophic cells) leads to chronic GH hypersecretion. Lower fat mass (with decreased adipocyte fat content and area) and hepatomegaly (with reduced liver fat) manifest in these transgenic mice (Abboud et al., 2020). Altogether, this evidence highlights the untapped potential of GPR101 as a therapeutic target for treating obesity.

In addition to roles in controlling body weight and GH secretion, GPR101 is the receptor mediating the leukocyte-directed actions of N-3 docosapentaenoic acid-derived resolvin D5 (RvD5n-3 DPA) in inflammatory arthritis (Flak et al., 2020). So-called specialized pro-resolving mediators (SPMs) resolve inflammation to restore homeostasis and include resolvins as well as lipoxins and protectins. As metabolic inflammation (metaflammation) may be involved in insulin resistance, curtailing inflammation could be beneficial for obesity and T2D (Charles-Messance et al., 2020). Thus, that RvD5n-3 DPA is a GPR101 agonist highlights an additional route through which targeting this receptor could benefit these disorders.

To understand the function of GPR101, we generated a GPR101 knockout (KO) mouse and assessed the metabolic phenotype on chow (CD) or chronic high-fat diet (HFD) feeding. Mechanistically, we explored the effect of GPR101 deletion on hypothalamic gene expression and microglia and astrocyte numbers. The results from the study indicate augmented DIO and insulin resistance risk as well as altered POMC and inflammatory activation associated with GPR101 loss highlighting the potential of this receptor as a novel therapeutic target for appetite control and obesity.

2. Methods

2.1. Generation of GPR101 KO mouse

The C57BL/6NTac-*Gpr101*[em7036Tac] mouse line with a constitutive Knock-Out (KO) of the *Gpr101* gene was custom-engineered using CRISPR/Cas9-mediated genome editing by Taconic Biosciences (https://www.taconic.com/genetically-engineered-animal-models/knockout-

mice/). The NCBI transcript NM_001033360.3 formed the foundation for the targeting strategy. Deletion of exons 1 and 2 including approx. 1.5 kb of the promoter region resulted in the loss of function of the *Gpr101* gene by deleting the complete gene. We backcrossed the mouse line onto C57BL/6NTac and confirmed that GPR101 mRNA significantly decreased in our transcriptomic analysis of the hypothalamus of *Gpr101* KO mice (Fig. 1A). Mice were group-housed in individually ventilated cages (Kallnik et al., 2007) with water and standard mouse chow available *ad libitum* before the start of the experiment according to the directive 2010/63/EU. The care and use of animals and assays used in this study were approved and carried out according to the ARRIVE guidelines and the rules outlined by the ethical committees of the district government of Upper Bavaria (Regierung von Oberbayern) and the Helmholtz Zentrum München in Germany.

2.2. Experimental design and body weight analysis

All mice had access to standard chow up to the age of 7 weeks. At this time point, male mice were randomly selected from the wild-type littermate control ("WT") and the hemizygous *Gpr101* KO ("MUT") groups and were given access to 60% kcal from fat HFD (Research Diets, Inc.) until the end of the experiment. Fig. 1B depicts the experimental design used for this analysis. From the age of 11–23 weeks, all mice were phenotyped systematically in the German Mouse Clinic as described previously (Fuchs et al. 2009, 2018) and Supplementary Fig. S1 shows the pipeline. The testing details described here are for those assays where there were genotype-pertinent alterations. We compared male MUT and WT mice on either standard chow (CD) or HFD and Supplementary Table 1 shows the number of animals per group and age of testing for the different assays. The mice were weighed throughout the experimental timeline to determine their body weight evolution.

2.3. Open field

The 20-min Open Field (OF) test was carried out at 11 weeks of age using the ActiMot system (TSE, Germany) as described previously (Garrett et al., 2012; Holter et al., 2015). The arena was made of transparent and infra-red light-permeable acrylic with a smooth floor (internal measurements: 45.5 x 45.5 x 39.5 cm, illumination = 150 lux corners, 200 lux middle).

2.4. Indirect calorimetry in metabolic homecages (MHC)

At the age of 15 weeks, MHC locomotor activity (distance travelled) and exploration (rearing), gas exchange (oxygen consumption and carbon dioxide production, VCO2/VO2), energy expenditure (heat production, kJ/h/animal), food intake and substrate utilisation of single-caged mice was measured by indirect calorimetry in metabolic homecages (TSE, Germany, see: https://www.mousephenotype.org/impress/ProcedureInfo?action=list&procID=855&pipeID=14). The measurement commenced 5 h before lights off and finished 4 h after lights-on the next morning (21 h in total).

2.5. Body composition (qNMR lean/fat) and anatomical examination

Our whole body composition analyzer (Bruker MiniSpec LF 50) based on Time Domain Nuclear Magnetic Resonance (TD-NMR) provides a robust method for the measurement of lean tissue and body fat in live mice without anaesthesia. It uses TD-NMR signals from all protons in the entire sample volume and provides data on lean and fat mass. A physical examination was performed by a trained experimenter and involved a whole-body checkup for anatomical abnormalities in different organ systems including skin, coat, limbs, tail, ears, snout, head, paws, digits, nails, teeth, genitalia and mouth.
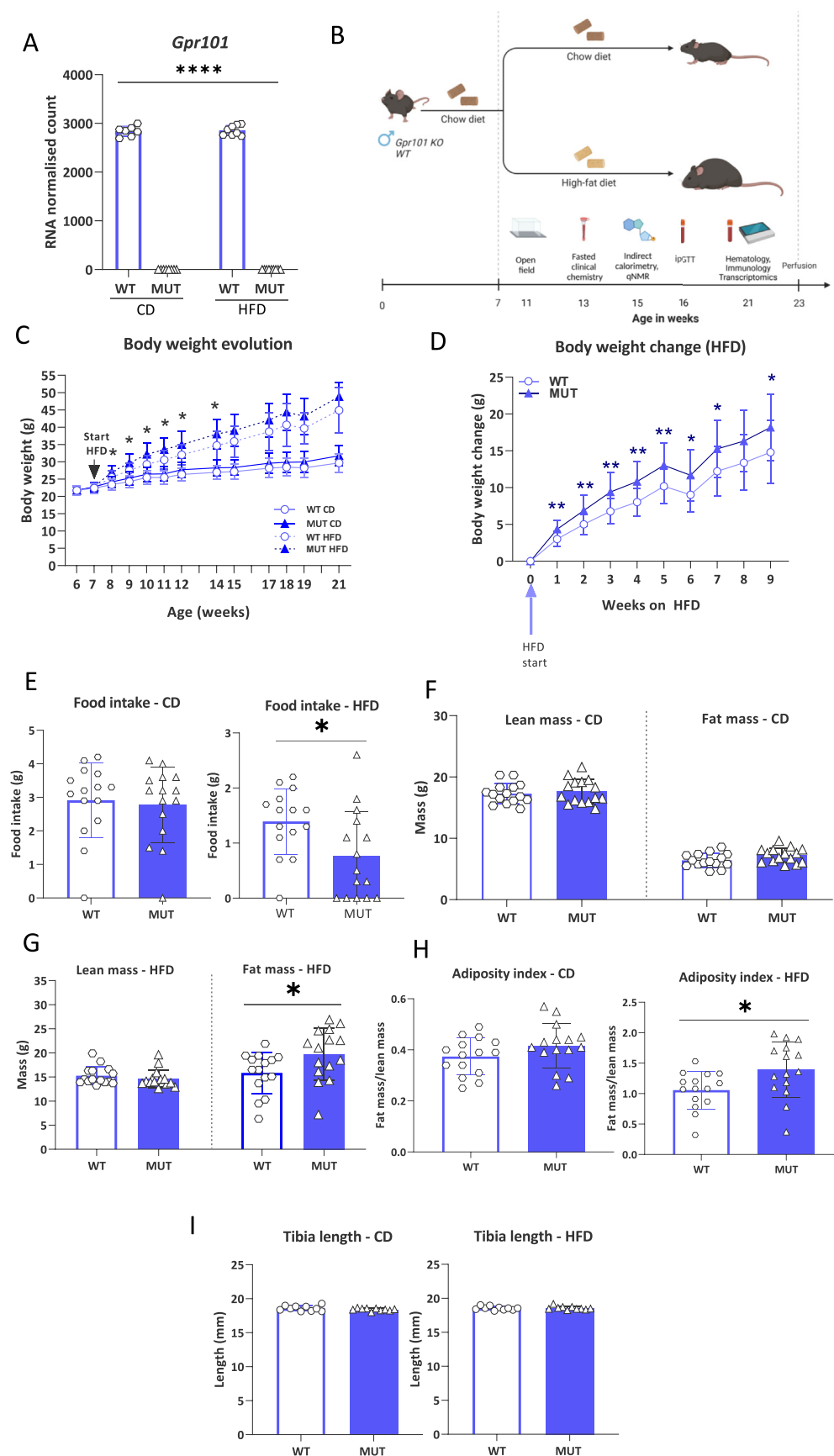
Fig. 1. Loss of *Gpr101* increased susceptibility to diet-induced obesity (DIO) on high-fat diet (HFD). Transcriptomic analysis of the hypothalamus revealed clear loss of *Gpr101* (**A**) in the mutant mice (MUT) compared to wild-type controls (WT) regardless of feeding with chow diet (CD) or HFD. ****p<0.0001 genotype effect in 2-way ANOVA. (**B**) The experimental design overview with the age at which the mice received HFD and the different assays performed (generated at www.biorender .com). WT and MUT mice consumed a 60% kcal HFD from the age of 7 weeks with a WT and MUT group remaining on CD. The body weight evolution over time for CD- and HFD-fed mice is shown in (**C**). The body weight change during initial weeks on HFD compared to starting body weight is displayed in (**D**). The food intake as measured during indirect calorimetry analysis at 15 weeks (**E**). The fat (**F**) and lean (**G**) mass were measured at the age of 15 weeks (8 weeks of HFD) as well as the adiposity index of fat mass (FM) in ratio to lean mass (LM) (**H**). The tibia length measurements are shown in (**I**). *p<0.05, **p<0.01, ****p<0.0001 WT vs. MUT. N = 15 per group for all measurements except n = 10 per group for tibia length.

2.6. Glucose tolerance test (GTT)

Glucose metabolism disturbance was determined using the (GTT) at the age of 16 weeks. Glucose was administered intraperitoneally (2 g/kg i. p.) after a 6-h food withdrawal and basal fasting glucose levels and 15, 30, 60, and 120 min after glucose injection were measured from a drop of blood collected from the tail vein with the Accu-Chek Aviva Connect glucose analyzer (Roche/Mannheim).

2.7. Blood collection, hematology and immunology

The final blood samples were collected under isoflurane anaesthesia by retrobulbar puncture in Li-heparin-coated tubes. They were then stored on ice until centrifugation (4500×g, 10 Min) and separation of plasma aliquots for further analyses. The clinical chemistry analyses of circulating biochemical parameters in *ad libitum* fed mouse blood was performed using a clinical chemistry analyser (Beckman Coulter AU 480 autoanalyzer, Krefeld, Germany) at the age of 21 weeks. A broad set of parameters was measured including enzyme activities as well as plasma concentrations of specific substrates and electrolytes (Rathkolb et al. 2013a, 2013b). Insulin, leptin and cytokine levels were measured with a combined electrochemiluminescence multiplex assay system (Meso Scale Discovery, MSD, Rockville, MD USA).

2.8. Pathological examination of the liver

For pathological analysis at 21 weeks of age, hematoxylin and eosin (H&E) staining was performed on formalin-fixed paraffin-embedded sections (4 μm) from the liver. Two independent pathologists analysed the slides according to standardized protocols as previously described (Fuchs et al., 2018).

2.9. RNA isolation and transcriptome analysis of hypothalamus

Hypothalami were dissected and total RNA was isolated using the RNeasy Mini kit (Qiagen) including Trizol treatment. The Agilent 2100 Bioanalyzer was used to assess RNA quality and RNA with RIN >7 was used for RNAseq analysis. Total RNA was analysed by RNA sequencing. Paired-end data was generated and analysed by a RNAseq pipeline consisting of quality control (FastQC, MultiQC), read trimming (trim_galore), genome alignment (STAR), and gene-level read counting (summarizeOverlaps, mode = 'Union'). The significantly regulated genes were determined with DEseq2 after excluding low expressed genes. For the biological interpretation of the observed gene regulation we performed protein-protein interaction analysis using the STRING ('Search Tool for Retrieval of Interacting Genes/Proteins') database, Version 11.5 (www.string-db.org) (Szklarczyk et al., 2019) and enrichment analyses with Enrichr (https://maayanlab.cloud/Enrichr/(Chen et al., 2013)). A microglia-specific enrichment analysis was also performed using MGEnrichment (https://ciernialab.shinyapps.io/MGEnrichmentApp/). This method entails the systematic association of the gene sets with biological terms to derive a mechanistic impression. While it will reveal whether gene subsets are relevant to a particular function or disease, further experimental validation is necessary to understand how specific genes affect the ascribed function. We used genome-wide transcriptome analysis on 17 KO animals (9 HFD, 8 CD) and 15 WT animals (8 HFD, 7 CD). All samples passed the quality control criteria and we conducted statistical analyses with DEseq2.

2.10. Tissue collection, immunostaining and design-based stereological analysis of microglia and astrocyte populations

Adult mice were euthanised and perfused by transcardial perfusion with a solution of 4% paraformaldehyde (PFA) in 0.1 M PBS (pH = 7.4). Dissected brains were post-fixed in the same fixative over night at 4 °C. Brains were transferred to a 30% (w/v) sucrose solution and stored at 4 °C 40 μm thick coronal sections were taken using a cryostat (Leica CM3050S), collected in cryoprotective solution (25% ethylene glycol and 25% glycerin in phosphate buffer) and stored at −20 °C. A one-in-six series of sections was used for each analysis.

For immunostaining of ionized calcium-binding adapter molecule 1 (IBA1)+ microglia and glial fibrillary acidic protein (GFAP)+ astrocytes, an Avidin-Biotin Complex (ABC) method like that employed previously (Garrett et al. 2018, 2020; Ung et al., 2021) was used. For IBA1 immunostaining, the antibodies used were a primary goat monoclonal anti-IBA1 antibody (Abcam plc, Cambridge, UK; order no ab5076; dilution 1:200) with a biotinylated rabbit anti-goat IgG (1:300 Biotin-SP AffiniPure Rabbit Anti-Goat IgG, Jackson ImmunoResearch Inc., USA). For GFAP immunostaining, a primary rabbit monoclonal anti-GFAP antibody (Abcam plc, Cambridge, UK; order no ab4648; dilution 1:5000) was implemented in conjunction with a biotinylated goat anti-rabbit IgG (1:300 Biotin-SP AffiniPure Goat Anti-Rabbit IgG, Jackson ImmunoResearch Inc., USA). The tertiary ABC complex was employed according to manufacturer's instructions (VECTASTAIN Elite ABC HRP Kit PK-6100, VECTOR LABORATORIES, INC., Burlingame, USA). The negative controls, with omission of the primary antibodies, revealed no positive staining.

A design-based unbiased stereology method was used to quantify IBA1+ and GFAP + cells in the ARC. We used StereoInvestigator software (MicroBrightField Biosciences Inc.) to estimate cell numbers (with optical fractionator). Optical fractionator is a method where the tissue volume fraction is implemented to determine a valid cell population number estimate within a given region (see Schmitz and Hof, 2005). The total number of cells (N) estimated is calculated using the following equation:

$$N = \sum Q^- x \left(\frac{1}{ssf}\right) x \left(\frac{1}{asf}\right) x \left(\frac{t}{h}\right)$$

Q is the total number of cells sampled, t is the section thickness, h is the dissector height, asf is the area sampling fraction and ssf is the section sampling fraction. We also measured the cell density as the number of cells per size-matched counting frame. The estimates were made in every sixth serial 40-μm coronal section as described previously (Heermann et al., 2019). The cells were visualized using a Zeiss microscope with a motorized stage coupled with a CCD colour camera to a computer. Systematic random sampling of every 6th section was undertaken through the ARC beginning at approximately bregma −1.22 mm, ending at approximately −2.54 mm according to the mouse brain atlas of Franklin and Paxinos (1997). The first sampled sections were chosen at random. Sections were cut at 40 μm giving approximately a 15-20-μm optical dissector height within each section after dehydration and mounting. Cells were counted using a systematic random grid overlay system controlled by the StereoInvestigator software in a previously outlined ARC region in all optical planes, generating a 3-dimensional counting area. Guard zones, where no cells are counted, were set at 10% of the section thickness to account for damage during the staining procedure and to prevent oversampling. Grid size and counting frame parameters were set to 100/100 μm. Using this frame area we could sample sufficient cells to achieve an acceptable Gunderson's coefficient of error (CE) below 0.1 with the smoothness factor m = 1. The CE estimates the sampling precision independent of biological variability. CE values closer to 0 have increased precision. Cells were only counted if they touched the inclusion border or did not touch the exclusion border of the counting frame. The observer was blind to the experimental groups. Two animals from each analysis were excluded due to tissue damaged during processing.

2.11. Microglial morphometric analysis

The branching morphology of the IBA1+ microglia was carried out as described previously (Ung et al., 2021) using a Zeiss Axio Imager M2 microscope (Carl Zeiss, Oberkochen, Germany) with a motorized stage and a CCD color camera and Neurolucida software (Version, 2018) and

Neurolucida Explorer (2018, MBF biosciences, Williston, VT, USA). Using the 100x objective, 5 microglial cells per animal were traced in the ARC between Bregma −1.22 to −2.54. Cell bodies of each cell were contoured in the Neurolucida program at the z-stage-level where it showed the biggest area in focus. The branches were traced in 3D focusing through the z-plane and adjusting for branch thickness. The traced 3D-cell structures were analysed in Neurolucida Explorer using the Branched Structure Analysis function. The parameters measured for each microglial cell were the number of endings, branch length and volume. The coefficient of variation within the morphological parameters for each animal was lower than 0.5.

2.12. Statistics

Data was analysed using either 2-way ANOVA with genotype and diet as main factors or with separate t-tests to determine genotype differences on CD or HFD. A *post-hoc* Fisher's LSD was used to test genotype x diet interaction effects. Whether the data assumed a normal Gaussian distribution was determined using the D'Agostino-Pearson test. A Grubb's test was used to identify outliers that were subsequently excluded from the analysis (1 WT on CD and 1 WT on HFD for insulin levels, 1 MUT on HFD for TNF removed). For body weight evolution, body weight change and ipGTT analysis, a repeated measures (RM) ANOVA (with post-hoc Sidak's test) was implemented with time and genotype/diet as independent variables. Data was statistically analysed using GraphPad Prism version 8 for Windows (GraphPad Software, La Jolla, California, USA, www.gra phpad.com). For all tests, a p value < 0.05 was the level of significance and data are mean ± SD. A correction for multiple testing was not performed.

2.13. Data availability

The RNA-seq data has been submitted to the GEO database at NCBI (GSE220533) and all phenotyping data will be available on the Pheno-map Viewer of the German Mouse Clinic webpage (http://tools.mouse clinic.de/phenomap/jsp/annotation/public/phenomap.jsf).

3. Results

3.1. GPR101 loss increases vulnerability to DIO

To determine whether constitutive loss of GPR101 (Fig. 1A shows downregulation of hypothalamic *Gpr101*) would increase vulnerability to DIO, we gave *Gpr101* young adult male hemizygous KO and control mice *ad libitum* access to 60% kcal from fat HFD over a period of 15–16 weeks from 7 weeks of age (Fig. 1B). The most notable phenotypes identified concerned the metabolism, clinical chemistry and immunology phenotype domains and minor changes in open field behavior as illustrated in the phenotypic profiles shown in Supplementary Fig. S3. Body weight measurements conducted over this period revealed that while a small increase in body weight was evident in the CD-fed MUT group, HFD consumption induced a more pronounced genotype difference as shown by the body weight evolution over time (Fig. 1C). This increased body weight was significant in the HFD-fed *Gpr101* mutant mice compared to controls during the first six weeks of HFD access (age 8–14 weeks). Nevertheless, there was higher within-group variation after this point and genotypic differences in absolute body weight diminished. This was reflected in the body weight change where the mutant mice initially gained significantly more weight compared to controls however the magnitude of this difference was not as pronounced from week 6 onwards (Fig. 1D). We observed a significant reduction in food intake in the mutant group after 8 weeks on HFD (15 weeks of age) not evident on CD (Fig. 1E). In particular, 5/15 mutant mice (compared to 1/15 control mice) did not consume HFD.

Using non-invasive quantitative nuclear magnetic resonance, we determined the body composition of fat and lean content (aged 15 weeks,

8 weeks HFD). While there were no genotype differences in fat or lean mass on CD (Fig. 1F), HFD increased the mutant fat mass without altering lean mass (Fig. 1G) and increased the adiposity index (fat mass/lean mass, Fig. 1H). Furthermore, in spite of GPR101 overexpression association with acromegaly, we did not detect anatomical alterations in *Gpr101* KO mice compared to control mice after physical examination. There were also no significant genotypic differences in mean tibia length (Fig. 1I).

### 3.2. GPR101 ablation causes hyperinsulinemia

To assess the effect of GPR101 loss on the glycemic index we measured circulating insulin, fasted glucose levels and glucose tolerance. Insulin resistance occurs when there is an impairment of the insulin influence on glucose metabolism. Hyperinsulinemia is then required to maintain signaling levels due to receptor downregulation and impaired glucose transport (Barazzoni et al., 2018). The *Gpr101* KO mice showed hyperinsulinemia compared to controls on both CD and HFD (Fig. 2A). To determine the association between this altered insulin state and effects on glucose regulation, we measured fasting glucose (after 6 weeks HFD) and performed the glucose tolerance test (ipGTT) after 10 weeks on HFD at 16 weeks of age. The loss of GPR101 slightly delayed glucose clearance on CD without differences on HFD (Fig. 2B) and did not alter circulating fasted glucose (Fig. 2C).

Reduced responsiveness to circulating insulin typifies insulin resistance and is a common feature of obesity that increases the risk of several pathological conditions, including hyperinsulinemia, glucose intolerance, T2D, cardiovascular disease and NAFLD. Indications of a risk towards the latter were suggested by the tendency to increased liver weight (body weight normalized), measured at the end of the study, with GPR101 loss and HFD feeding. Furthermore, qualitative analysis of H&E stained liver sections suggests an exacerbation of HFD-induced lipid accumulation with GPR101 loss (Fig. 2D and E).
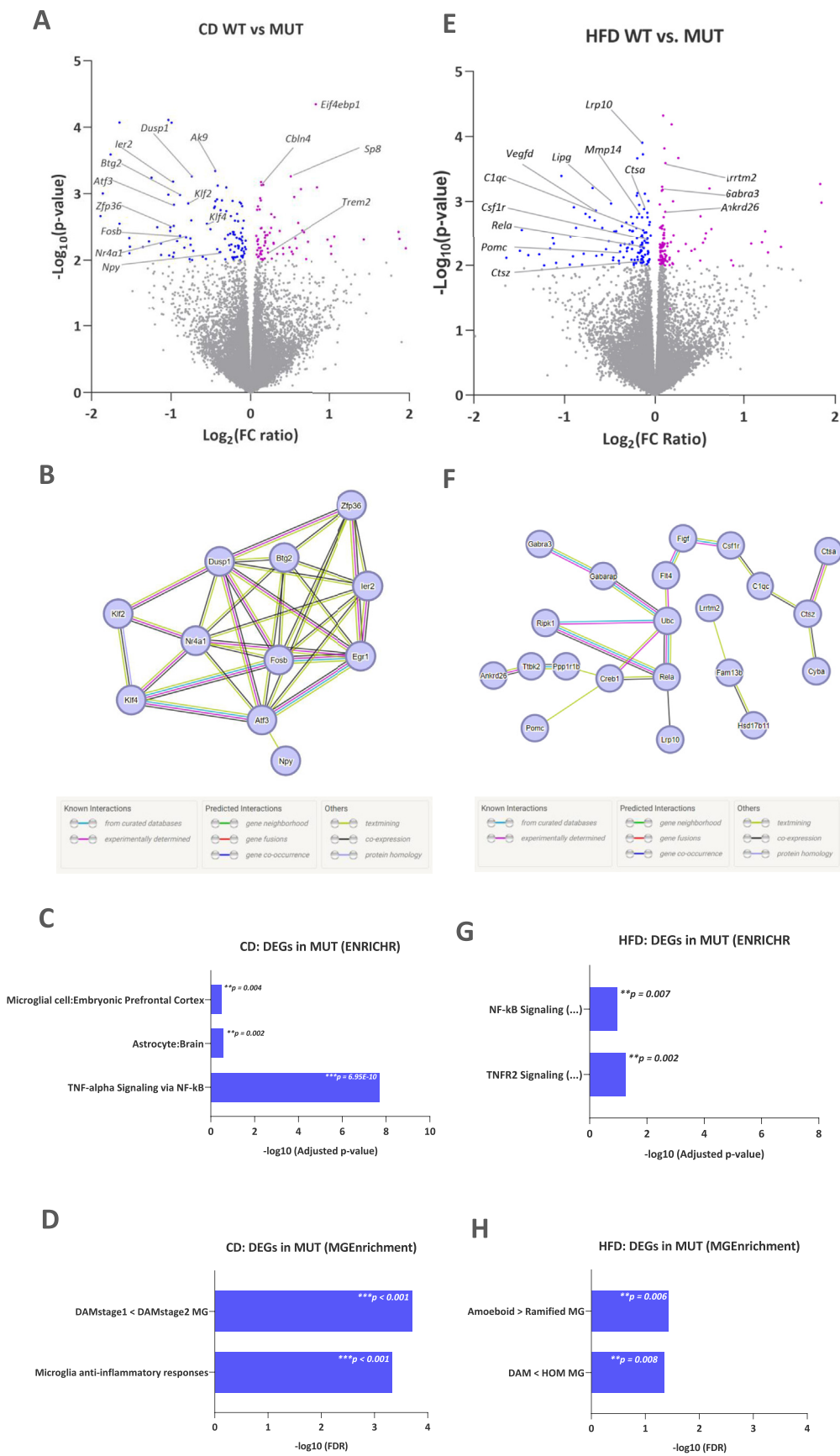
3.3. GPR101 loss alters hypothalamic immuno-regulatory gene expression

Given the hypothalamic GPR101 expression and that HFD-induced gliosis and metabolic stress lead to hypothalamic circuit dysfunction (De Souza et al., 2005; Kothari et al., 2017), we performed RNA-Seq analysis of this region to investigate the molecular basis for the GPR101 loss-associated increased DIO risk (in 21-week-old mice, 15 weeks HFD, full gene lists in Supplementary information gene lists).

CD: We observed 179 differentially expressed genes (DEGs) in mutant mice compared to controls on CD (Fig. 3A). The strongest were associated with immune regulation and microglial activity. This included upregulation of the disease-associated microglia (DAM) gene *Trem2* (Triggering receptor expressed on myeloid cells 2) (Fig. 3A). It is expressed predominantly in brain microglia, playing an immune homeostatic role, necessary for microglial proliferation, migration, phagocytosis, cytokine release, lipid sensing and ApoE binding (Atagi et al., 2015; Kleinberger et al., 2014; Ulrich and Holtzman 2016). Upregulation of hypothalamic TREM2 suggests potential immune activation. Accordingly, this was accompanied by downregulation of the gene encoding ZFP36 (Zinc-finger protein 36 or Tristetraprolin (TTP)) and the related protein functional interaction network (Fig. 3A and B, *Zfp36, Btg2, Dusp1, Nr4a1, Egr1, Fosb, Klf4, Klf2, Atf3* and *Ier2*, Table 1 for functional annotations). TTP is an RNA-binding protein controlling RNA stability and is anti-inflammatory by guiding unstable pro-inflammatory protein mRNA. TTP loss thereby has the potential to elevate TNF-α cytokine expression and enhance hypothalamic inflammation through activating microglia (as is evidenced here by *Trem2* upregulation) altering energy expenditure (Jeong et al., 2021). This is confirmed by the enrichment of the terms "*TNF alpha Signaling by NF-kB*", "*Astrocyte:Brain*" and "*Microglial cell: embryonic prefrontal cortex*" for these DEGs (Fig. 3C, see Supplementary Information for full enrichment details). A microglia (MG)-specific enrichment analysis (MGEnrichment (Jao and Ciernia 2021), Fig. 3D,
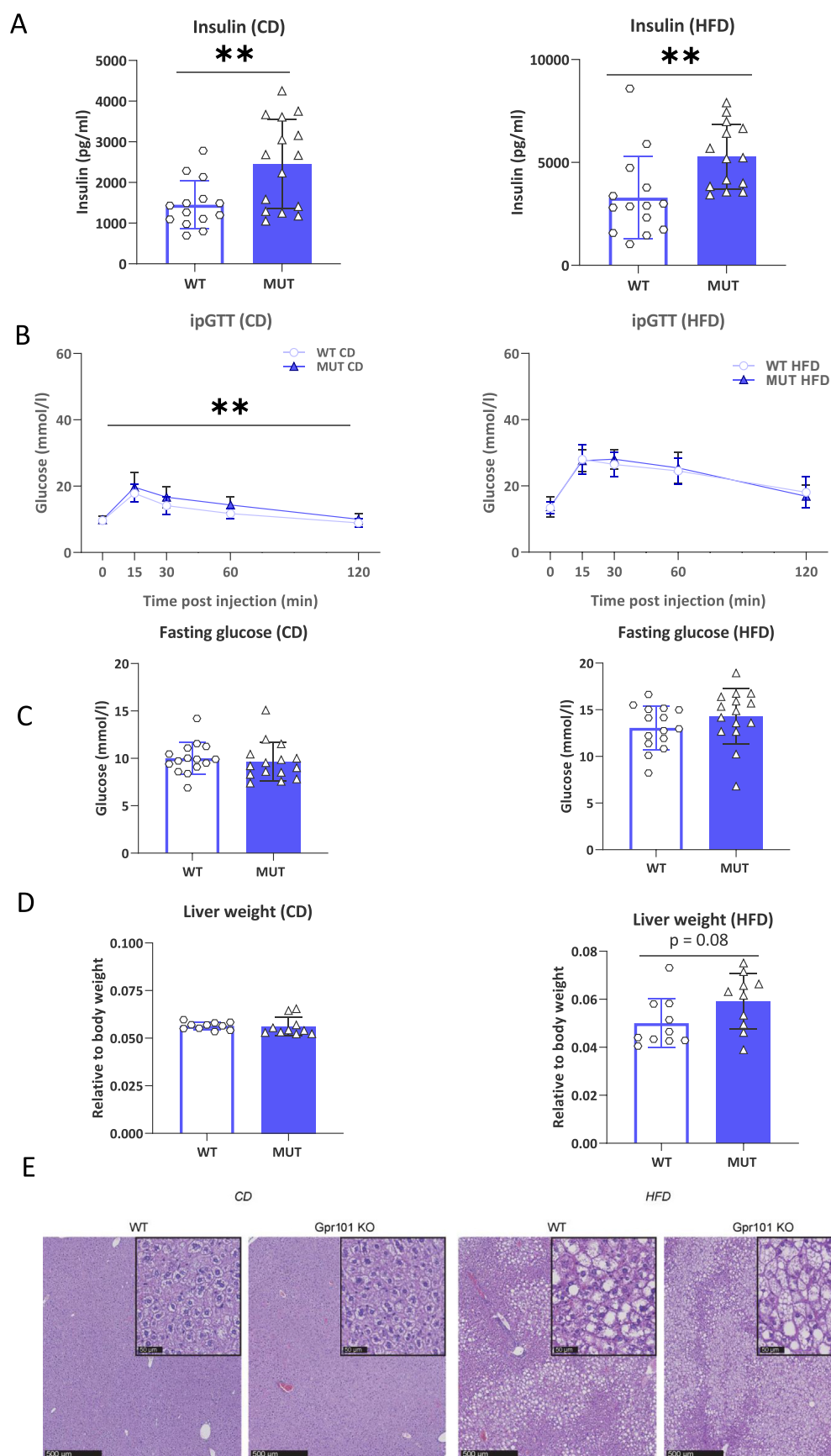
Fig. 2. Loss of *Gpr101* increased insulin resistance risk and impaired glucose clearance. Circulating plasma insulin levels of *Gpr101* (MUT) with high-fat diet (HFD) and without (CD – chow diet) compared to wildtype controls (WT) n = 14 WT (CD, HFD), n = 15/14 MUT (CD/HFD) (**A**). Glucose levels during the intraperitoneal glucose tolerance test (ipGTT), used to assess glucose clearance after i. p. injection of a glucose bolus n = 15 per group (**B**). The fasting glucose levels are shown n = 15 per group (**C**). Body weight normalized liver weight (**D**) and hematoxylin and eosin stained liver sections n = 10 per group (**E**). **p < 0.01, MUT vs. WT.

A CD WT vs MUT

E HFD WT vs. MUT

B

F

C CD: DEGs in MUT (ENRICHR)

G HFD: DEGs in MUT (ENRICHR

D CD: DEGs in MUT (MGEnrichment)

H HFD: DEGs in MUT (MGEnrichment)

(caption on next page)

Fig. 3. GPR101 loss induced aberrant hypothalamic expression of inflammation, microglial and feeding-related genes with and without high-fat diet challenge. Transcriptomic analysis of hypothalamus revealed differentially expressed genes (DEGs) from *Gpr101* knockout ("MUT") and control ("WT") mice on either standard chow-diet (CD) or 60% kcal high-fat diet (HFD) from 21-week old mice after 15 weeks HFD. (**A**) Volcano plot showing significantly (p < 0.01) up- (magenta points) and down- (blue points) regulated genes in MUT vs. WT mice on CD (FC = fold change). (**B**) A STRING (Search Tool for the Retrieval of Interacting Genes/ Proteins) predicted functional association network DEGs in MUT mice on CD with the main evidence for protein-protein interactions (PPIs) depicted. The legend (taken from string-db.org) is also shown. Each node is representative of all proteins produced by a protein coding gene. The edges indicate protein-protein associations with shared functions. Magenta- and cyan-colored edges are established interactions and the remainder are predicted interactions. There was a significant PPI network for the ZFP36/Tristetraprolin (TTP) protein (related nodes highlighted in purple), the downregulation of which is associated with increased inflammation. Depicted are selected significant terms from the enrichment analysis of the MUT DEGs on CD using the *Enrichr* platform accessing different databases (https://maayanlab.cloud /Enrichr/) (**C**) and with the microglia-specific MGEnrichment analysis tool (https://ciernialab.shinyapps.io/MGEnrichmentApp/) (**D**). (**E-H**) Volcano plot, STRING, ENRICHR and MGEnrichment analysis of MUT DEGs on HFD. There was differential regulation of genes involved in glutamatergic (*Lrrtm2*) and GABAergic (*Gabra3*) signaling, appetite (*Ankrd26, Pomc*), inflammation and microglia (*Rela, Csf1r, C1qc, Ubc, Ripk1*), endothelial cell signaling (*Vegfd* (*Figf*), *Vegfr3* (*Flt4*)), phagocytosis (*Gabarap, Cyba*) and lipid metabolism (*Lrp10*). Selected significant enriched terms from the enrichment analysis with Enrichr and MGEnrichment are shown. FDR = false discovery rate. The raw p values and significance are depicted in the respective bar. *p<0.05, **p<0.01, ***p <0.001. (For interpretation of the references to color in this figure legend, the reader is referred to the Web version of this article.)

and Supplementary information) showed enrichment of the terms: "*DAMstage1* < *DAMstage2 MG*" and "*Microglia anti-inflammatory responses*". This infers that loss of GPR101 on CD induces a hypothalamic molecular signature characteristic of stage 2 DAMs (rather than stage 1) and altered microglial anti-inflammatory responsivity. DAMs are produced through a two-step mechanism (Keren-Shaul et al., 2017) transitioning from the resting/homeostatic microglial state to an intermediate (stage 1) and then to a TREM2-dependent activation state (stage 2). This evolution includes upregulation of *Trem2* and downregulation of the anti-inflammatory TTP interactome genes, consistent with the hypothalamic DEG pattern observed with GPR101 loss under standard conditions.

HFD: There were 227 DEGs in mutant mice compared to controls on HFD (Fig. 3E and F, with raw *P* < 0.01, not significant with *P*adj). The prevailing pattern again indicates differential regulation of immune and microglial activity (*Rela, Csf1r, C1qc, Gabarap, Cyba*)-related genes among others (endothelial cell: *Vegf3* (*Figf*), *Vegfr-3* (*Flt4*)), excitation/ inhibition: (*Gabra3* [GABAergic receptor subunit alpha-3 gene], *Lrrtm2* [Leucine-rich repeat transmembrane neuronal protein-2]). Appetite, phagocytosis and lipid metabolism (*Pomc, Ankrd26* [Ankyrin repeat domain 26], *Lrp10, Gabarap, Cyba*)-related genes were also altered. *Lrp10* (low-density lipoprotein receptor-related protein 10) mediates internalization of lipophilic ApoE implicated in cholesterol efflux and microglial phagocytosis (Gibbons et al., 2010)·(Jeong et al., 2019). Impaired autophagy, as indicated by downregulated *Gabarap* and *Cyba*, can lead to changes in lipid metabolism (Saito et al., 2019). The immunoregulatory terms "*TNFR2 signaling*" and "*NF-kB signaling*" were enriched within the HFD DEGs (Fig. 3G) as were the microglial terms "*Amoeboid > Ramified MG*" and "*DAM < HOM MG*" (Fig. 3H). This suggests that GPR101 loss on HFD produces a molecular signature consistent with altered DAM activation ("*DAM < HOM MG*") and a shift between ramified and amoeboid microglial morphology indicative of a modified phagocytic state. Overall, this transcriptomic evidence indicates that loss of GPR101 leads to altered hypothalamic microglial phagocytosis and impaired lipid metabolism after 15 weeks on HFD. Neither *Gh* nor its receptors were differentially regulated in the hypothalamus with GPR101 loss (Supplementary Fig. S3).

3.4. GPR101 loss alters immune markers and hypothalamic microglial morphology

Based on the transcriptomic analysis, we performed a more detailed investigation of inflammatory markers as well as microglia and astrocyte cell populations in the ARC of the hypothalamus. Inflammation is causally linked to obesity and obesity-associated disorders, e.g. systemic insulin resistance and NAFLD due to chronic activation of stress- and inflammation-related kinases (Donath and Shoelson, 2011; Lumeng and Saltiel, 2011). GPR101 loss on HFD feeding induced innate immune response activation that was not evident with intact functioning of this protein on the same diet. This was manifest as increased circulating

monocyte ((Fig. 4A) and TNF-α (Fig. 4B) levels in the mutant mice.

We used design-based stereology to quantify microglial (IBA1+) and astrocyte (GFAP+) cell density and microglial morphometry to index microglial activation. Our analysis revealed that astrocyte density increased on HFD with no apparent influence of GPR101 loss (Fig. 4C and D). Furthermore, while HFD did not significantly alter microglia density at this time point (23 weeks of age, 16 weeks HFD), loss of GPR101 function increased microglia density in the ARC (Fig. 4E and F). As described, the MGEnrichment analysis revealed GPR101 loss caused differential regulation of genes affecting amoeboid microglial morphology formation. When activated, the microglial cell soma is enlarged and less ramified with shorter branches yielding an amoeboid appearance, emblematic of ongoing phagocytosis (Morrison and Filosa 2013). Previous evidence shows that hypothalamic ARC microglia increase in size with 16 weeks HFD (Valdearcos et al., 2014). Nevertheless, GPR101 deficient mice exhibited more elongated ramified ARC microglia on HFD compared to CD (Fig. 4G and H), with increased branch number ("Ends", Fig. 4H), volume (Fig. 4H) and branch length (Fig. 4H). The latter tended to be increased compared to WT on HFD and this pattern was not evident in mice with functioning GPR101 (Fig. 4H). Overall, the morphology indicates that GPR101 deficient microglia are enlarged and exhibit impaired phagocytosis in response to HFD.

4. Discussion

The oGPCR GPR101 is a promising target for metabolic disease treatment due to expression in brain regions controlling energy homeostasis (Bates et al., 2006; Nilaweera et al., 2007). To elucidate further the function and role of this receptor in energy balance regulation, we scrutinized a *Gpr101* full knockout mouse line (hemizygous males) under both standard and chronic HFD feeding conditions. Building on the extant correlational mouse (Nilaweera et al., 2007) and human data (Akiyama et al., 2017), we showed that *Gpr101* loss heightened DIO risk during HFD challenge with a persistent body composition shift to increased adiposity. Moreover, there was genotype-dependent hyperinsulinemia (with and without HFD) and reduced glucose tolerance (on CD), hinting toward increased insulin resistance in mutants. Our hypothalamic transcriptomic analysis indicated that constitutive loss of GPR101 alters feeding, lipid metabolism, microglial and inflammation-associated gene activation both under balanced and HFD conditions. This was coupled with aberrant surrogate indices of hypothalamic microglial activity that likely, among other factors, contributed to the heightened DIO risk. Consonant with the pleiotropy and ability of GPCRs to respond to multiple ligands, there are potentially several underlying factors involved (discussed below) (Wacker et al., 2017).

Direct effects of GPR101 loss on the hypothalamic neurons mediating feeding and energy homeostasis can contribute to the associated DIO risk. Existing correlational data implicates GPR101 in appetite and feeding regulation (Nilaweera et al., 2007). Expressed in a subset of anorexigenic POMC+ (~55%) and orexigenic NPY+ (5%) neurons (Nilaweera et al.,

Table 1

Protein annotations of selected hypothalamic differentially expressed genes with GPR101 loss and high-fat diet feeding. From https://string-db.org.

Gene	Protein annotation
Btg2	BTG2; Anti-proliferative protein; the function is mediated by association with deadenylase subunits of the CCR4-NOT complex. Activates mRNA deadenylation in a CNOT6 and CNOT7-dependent manner. In vitro can inhibit deadenylase activity of CNOT7 and CNOT8. Involved in cell cycle regulation. Could be involved in the growth arrest and differentiation of the neuronal precursors. Modulates transcription regulation mediated by ESR1. Involved in mitochondrial depolarization and neurite outgrowth (By similarity); Belongs to the BTG family (158 aa)
Ccl12	C–C motif chemokine 12; Chemotactic factor that attracts eosinophils, monocytes, and lymphocytes but not neutrophils. Potent monocyte active chemokine that signals through CCR2. Involved in allergic inflammation and the host response to pathogens and may play a pivotal role during early stages of allergic lung inflammation; Belongs to the intercrine beta (chemokine CC) family (104 aa)
Klf2	Kruppel-like factor 2 (lung); Krueppel-like factor 2; Transcription factor that binds to the CACCC box in the promoter of target genes such as HBB/beta globin or NOV and activates their transcription (354 aa)
Hist1h4j	H4 clustered histone 6; Histone cluster 1, H4j; Core component of nucleosome. Nucleosomes wrap and compact DNA into chromatin, limiting DNA accessibility to the cellular machineries which require DNA as a template. Histones thereby play a central role in transcription regulation, DNA repair, DNA replication and chromosomal stability. DNA accessibility is regulated via a complex set of post-translational modifications of histones, also called histone code, and nucleosome remodeling (103 aa)
Atf3	Cyclic AMP-dependent transcription factor ATF-3; This protein binds the cAMP response element (CRE) (consensus: 5′-GTGACGT[AC][AG]-3′), a sequence present in many viral and cellular promoters. Represses transcription from promoters with ATF sites. It may repress transcription by stabilizing the binding of inhibitory cofactors at the promoter (By similarity); Belongs to the bZIP family. ATF subfamily (181 aa)
Nr4a1	Nuclear receptor subfamily 4, group a, member 1; Nuclear receptor subfamily 4 group A member 1; Orphan nuclear receptor. May act concomitantly with NURR1 in regulating the expression of delayed-early genes during liver regeneration. Binds the NGFI-B response element (NBRE) 5′- AAAAGGTCA-3'. May inhibit NF-kappa-B transactivation of IL2. Participates in energy homeostasis by sequestering the kinase STK11 in the nucleus, thereby attenuating cytoplasmic AMPK activation (By similarity) (601 aa)
Fseg	DEPP1 autophagy regulator; Protein DEPP1; Acts as a critical modulator of FOXO3-induced autophagy via increased cellular ROS (205 aa)
Klf4	Krueppel-like factor 4; Transcription factor; can act both as activator and as repressor. Binds the 5′-CACCC-3′ core sequence. Binds to the promoter region of its own gene and can activate its own transcription. Regulates the expression of key transcription factors during embryonic development. Plays an important role in maintaining embryonic stem cells, and in preventing their differentiation. Required for establishing the barrier function of the skin and for postnatal maturation and maintenance of the ocular surface. Involved in the differentiation of epithelial cells (483 aa)
Cytip	Cytohesin-interacting protein; By its binding to cytohesin-1 (CYTH1), it modifies activation of ARFs by CYTH1 and its precise function may be to sequester CYTH1 in the cytoplasm (359 aa)
Gpr101	Probable G-protein coupled receptor 101; Orphan receptor (511 aa)
Ier2	Immediate early response gene 2 protein; DNA-binding protein that seems to act as a transcription factor (By similarity). Involved in the regulation of neuronal differentiation, acts upon JNK-signaling pathway activation and plays a role in neurite outgrowth in hippocampal cells (By similarity). May mediate with FIBP FGF-signaling in the establishment of laterality in the embryo (By similarity). Promotes cell motility, seems to stimulate tumor metastasis (By similarity) (221 aa)
Dusp1	Dual specificity protein phosphatase 1; Dual specificity phosphatase that dephosphorylates MAP kinase MAPK1/ERK2 on both 'Thr-183' and 'Tyr-185', regulating its activity during the meiotic cell cycle; Belongs to the protein-tyrosine phosphatase family. Non-receptor class dual specificity subfamily (367 aa)
C1qtnf3	Complement c1q tumor necrosis factor-related protein 3; C1q and tumor necrosis factor related protein 3 (319 aa)
Egr1	Early growth response protein 1; Transcriptional regulator. Recognizes and binds to the DNA sequence 5′-GCG(T/G)GGGCG-3′(EGR-site) in the promoter region of target genes. Binds double-stranded target DNA, irrespective of the cytosine methylation status (By similarity). Regulates the transcription of numerous target genes, and thereby plays an important role in regulating the response to growth factors, DNA damage, and ischemia. Plays a role in the regulation of cell survival, proliferation and cell death. Activates expression of p53/TP53 and TGFB1, and thereby helps prevent tumor formation (533 aa)
Cdc20b	Cell division cycle 20B (519 aa)
Fosb	Fbj osteosarcoma oncogene b; Protein fosB; FosB interacts with Jun proteins enhancing their DNA binding activity; Belongs to the bZIP family. Fos subfamily (338 aa)
Scin	Adseverin; Ca(2+)-dependent actin filament-severing protein that has a regulatory function in exocytosis by affecting the organization of the microfilament network underneath the plasma membrane. Severing activity is inhibited by phosphatidylinositol 4,5-bis-phosphate (PIP2) (By similarity). In vitro, also has barbed end capping and nucleating activities in the presence of Ca(2+). Required for megakaryocyte differentiation, maturation, polyploidization and apoptosis with the release of platelet-like particles (By similarity). Plays a role in osteoclastogenesis (OCG) (715 aa)
9530053A07Rik	RIKEN cDNA 9530053A07 gene (2581 aa)
Zfp36	mRNA decay activator protein ZFP36; Zinc-finger RNA-binding protein that destabilizes numerous cytoplasmic AU-rich element (ARE)-containing mRNA transcripts by promoting their poly(A) tail removal or deadenylation, and hence provide a mechanism for attenuating protein synthesis. Acts as an 3′-untranslated region (UTR) ARE mRNA-binding adapter protein to communicate signaling events to the mRNA decay machinery. Recruits deadenylase CNOT7 (and probably the CCR4-NOT complex) via association with CNOT1, and hence promotes ARE-mediated mRNA deadenylation. (319 aa)
Aipl1	Aryl-hydrocarbon-interacting protein-like 1; May be important in protein trafficking and/or protein folding and stabilization (328 aa)
E2f8	Transcription factor E2F8; Atypical E2F transcription factor that participates in various processes such as angiogenesis and polyploidization of specialized cells. Mainly acts as a transcription repressor that binds DNA independently of DP proteins and specifically recognizes the E2 recognition site 5′-TTTC[CG]CGC-3'. Directly represses transcription of classical E2F transcription factors such as E2F1: component of a feedback loop in S phase by repressing the expression of E2F1, thereby preventing p53/TP53-dependent apoptosis. Plays a key role in polyploidization of cells in placenta (860 aa)
Ssx9	MCG116991, isoform CRA_b; Synovial sarcoma, X breakpoint 9 (170 aa)
Apold1	Apolipoprotein L domain containing 1 (246 aa)
Ccna2	Cyclin-A2; Cyclin which controls both the G1/S and the G2/M transition phases of the cell cycle. Functions through the formation of specific serine/threonine kinase holoenzyme complexes with the cyclin-dependent protein kinases CDK1 and CDK2. The cyclin subunit confers the substrate specificity of these complexes and differentially interacts with and activates CDK1 and CDK2 throughout the cell cycle (422 aa)
Kri1	KRI1 homolog (S. cerevisiae); Belongs to the KRI1 family (705 aa)
D630003M21Rik	Uncharacterized protein KIAA1755 homolog; RIKEN cDNA D630003M21 gene (1187 aa)
Gpr101	Probable G-protein coupled receptor 101; Orphan receptor (511 aa)
Pgap1	Post-gpi attachment to proteins 1; GPI inositol-deacylase; Involved in inositol deacylation of GPI-anchored proteins. GPI inositol deacylation may important for efficient transport of GPI-anchored proteins from the endoplasmic reticulum to the Golgi (By similarity) (922 aa)
Dnm1l	Dynamin-1-like protein; Functions in mitochondrial and peroxisomal division. Mediates membrane fission through oligomerization into membrane- associated tubular structures that wrap around the scission site to constrict and sever the mitochondrial membrane through a GTP hydrolysis-dependent mechanism. Through its function in mitochondrial division, ensures the survival of at least some types of postmitotic neurons, including Purkinje cells, by suppressing oxidative damage. Required for normal brain development, including that of cerebellum. Facilitates developmentally regulated apoptosis (716 aa)
Acsbg1	Acyl-coa synthetase bubblegum family member 1; Long-chain-fatty-acid–CoA ligase ACSBG1; Mediates activation of long-chain fatty acids for both synthesis of cellular lipids, and degradation via beta-oxidation. Able to activate long-chain fatty acids. Can activate diverse saturated, monosaturated and polyunsaturated fatty acids (By similarity) (721 aa)
Elavl4	ELAV-like protein 4; May play a role in neuron-specific RNA processing. Protects CDKN1A mRNA from decay by binding to its 3′-UTR. Binds to AU-rich sequences (AREs) of target mRNAs, including VEGF and FOS mRNA (By similarity) (385 aa)

Table 1 (*continued*)

Gene	Protein annotation
Pak3	Serine/threonine-protein kinase PAK 3; Serine/threonine protein kinase that plays a role in a variety of different signaling pathways including cytoskeleton regulation, cell migration, or cell cycle regulation. Plays a role in dendrite spine morphogenesis as well as synapse formation and plasticity. Acts as downstream effector of the small GTPases CDC42 and RAC1. Activation by the binding of active CDC42 and RAC1 results in a conformational change and a subsequent autophosphorylation on several serine and/or threonine residues. Phosphorylates MAPK4 and MAPK6 (544 aa)
Zfp64	Zinc finger protein 64, isoform cra_b; May be involved in transcriptional regulation (676 aa)
Hr	Lysine demethylase and nuclear receptor corepressor; Lysine-specific demethylase hairless; Histone demethylase that specifically demethylates both mono- and dimethylated 'Lys-9′ of histone H3. May act as a transcription regulator controlling hair biology (via targeting of collagens), neural activity, and cell cycle (By similarity) (1182 aa)
Kcne1l	Potassium voltage-gated channel, isk-related family, member 1-like, pseudogene; Potassium voltage-gated channel subfamily E regulatory beta subunit 5; Potassium channel ancillary subunit that is essential for generation of some native K(+) currents by virtue of formation of heteromeric ion channel complex with voltage-gated potassium (Kv) channel pore-forming alpha subunits. Functions as an inhibitory beta-subunit of the repolarizing cardiac potassium ion channel KCNQ1 (143 aa)
Lrrtm2	Leucine-rich repeat transmembrane neuronal protein 2; Involved in the development and maintenance of excitatory synapse in the vertebrate nervous system. Regulates surface expression of AMPA receptors and instructs the development of functional glutamate release sites. Acts as a ligand for the presynaptic receptors NRXN1-A and NRXN1-B (By similarity) (515 aa)
Ctsa	Cathepsin a (carboxypeptidase c); Lysosomal protective protein; Protective protein appears to be essential for both the activity of beta-galactosidase and neuraminidase, it associates with these enzymes and exerts a protective function necessary for their stability and activity. This protein is also a carboxypeptidase and can deamidate tachykinins (474 aa)
Car3	Carbonic anhydrase 3; Reversible hydration of carbon dioxide (260 aa)
Prrg3	Proline rich Gla (G-carboxyglutamic acid) 3 (transmembrane) (231 aa)
Mmp14	Matrix metalloproteinase-14 (membrane-inserted); Matrix metalloproteinase-14; Endopeptidase that degrades various components of the extracellular matrix such as collagen. Activates progelatinase A. Essential for pericellular collagenolysis and modeling of skeletal and extraskeletal connective tissues during development. May be involved in actin cytoskeleton reorganization by cleaving PTK7 (By similarity). Acts as a positive regulator of cell growth and migration via activation of MMP15. Involved in the formation of the fibrovascular tissues (By similarity). (582 aa)
Figf	Vascular endothelial growth factor D; Growth factor active in angiogenesis, lymphangiogenesis and endothelial cell growth, stimulating their proliferation and migration and also has effects on the permeability of blood vessels. May function in the formation of the venous and lymphatic vascular systems during embryogenesis, and also in the maintenance of differentiated lymphatic endothelium in adults. Binds and activates VEGFR-3 (Flt4) receptor (358 aa)
Tmem80	Transmembrane protein 80 (123 aa)
Alox12b	Arachidonate 12-lipoxygenase, 12R-type; Non-heme iron-containing dioxygenase that catalyzes the stereo-specific peroxidation of free and esterified polyunsaturated fatty acids generating a spectrum of bioactive lipid mediators. Mainly converts arachidonic acid to (12R)- hydroperoxyeicosatetraenoic acid/ (12R)-HPETE and minor stereoisomers. In the skin, acts upstream of ALOXE3 on the lineolate moiety of esterified omega-hydroxyacyl-sphingosine (EOS) ceramides to produce an epoxy-ketone derivative, a crucial step in the conjugation of omega-hydroxyceramide to membrane proteins. (701 aa)
Gabra3	Gamma-aminobutyric acid receptor subunit alpha-3; GABA, the major inhibitory neurotransmitter in the vertebrate brain, mediates neuronal inhibition by binding to the GABA/benzodiazepine receptor and opening an integral chloride channel; Belongs to the ligand-gated ion channel (TC 1.A.9) family. Gamma-aminobutyric acid receptor (TC 1.A.9.5) subfamily. GABRA3 sub-subfamily (492 aa)
Crebrf	CREB3 regulatory factor; Acts as a negative regulator of the endoplasmic reticulum stress response or unfolded protein response (UPR). Represses the transcriptional activity of CREB3 during the UPR. Recruits CREB3 into nuclear foci (By similarity) (640 aa)
Ramp1	Receptor activity-modifying protein 1; Transports the calcitonin gene-related peptide type 1 receptor (CALCRL) to the plasma membrane. Acts as a receptor for calcitonin-gene-related peptide (CGRP) together with CALCRL; Belongs to the RAMP family (148 aa)
Morc4	MORC family CW-type zinc finger protein 4; Microrchidia 4 (883 aa)
Lipg	Endothelial lipase; Has phospholipase and triglyceride lipase activities. Hydrolyzes high density lipoproteins (HDL) more efficiently than other lipoproteins. Binds heparin (By similarity) (500 aa)
Agpat4	1-acylglycerol-3-phosphate O-acyltransferase 4 (lysophosphatidic acid acyltransferase, delta); 1-acyl-sn-glycerol-3-phosphate acyltransferase delta; Converts lysophosphatidic acid (LPA) into phosphatidic acid by incorporating an acyl moiety at the sn-2 position of the glycerol backbone; Belongs to the 1-acyl-sn-glycerol-3-phosphate acyltransferase family (378 aa)
Lrp10	Low-density lipoprotein receptor-related protein 10; Probable receptor, which is involved in the internalization of lipophilic molecules and/or signal transduction. May be involved in the uptake of lipoprotein APOE in liver (713 aa)
Ankrd26	Ankyrin repeat domain 26; Acts as a regulator of adipogenesis. Involved in the regulation of the feeding behavior (1681 aa)
Npepl1	Probable aminopeptidase NPEPL1; Probably catalyzes the removal of unsubstituted N- terminal amino acids from various peptides (524 aa)
Cpm	Carboxypeptidase M; Specifically removes C-terminal basic residues (Arg or Lys) from peptides and proteins. It is believed to play important roles in the control of peptide hormone and growth factor activity at the cell surface, and in the membrane-localized degradation of extracellular proteins (By similarity) (443 aa)
Prpf40b	Pre-mRNA-processing factor 40 homolog B; May be involved in pre-mRNA splicing; Belongs to the PRPF40 family (873 aa)

2007), activation putatively facilitates the release of the melanocortins α-, β- and γ-melanocyte stimulating hormone (MSH) suppressing appetite (Bagnol 2010). That GPR101 ablation decreased hypothalamic *Pomc* activation on HFD likely undermined this response promoting hunger and feeding. The reduced food intake at 8 weeks on HFD may be a behavioral reaction to the novel and relatively short-term exposure (21h) to the metabolic home cage environment. Alternatively, an initial increased HFD feeding can be blunted over time by parallel alterations suggested by the hypothalamic transcriptomic profile. For example, the upregulation of the GABAergic receptor subunit *Gabra3* and the gluta-matergic AMPA receptor-anchoring *Lrrtm2* indicates changes in inhibitory and excitatory function. It is thus relevant, for example, that in the POMC/GABAergic neuron subset, *Pomc* expression restores normal food intake in obese mice that could be assessed using POMC + cell-specific *Gpr101* KO mice (Trotta et al., 2020) (Steuernagel et al., 2022). In addition, ANKRD26 regulates adipogenesis and disruption in mice caused obesity, insulin resistance and increased feeding behaviour putatively through primary ciliopathy of the melanocortin pathway neurons (Acs et al., 2015; Bera et al., 2008). Increased ANKRD26 activation

therefore potentially offsets the effects of GPR101 loss on feeding and metabolic regulation for confirmation in future studies. Altered GH signalling due to GPR101 loss may also contribute to fat accumulation and hyperinsulinemia (Sharma et al., 2018) (Abboud et al., 2020; Rodd et al., 2016; Sharma et al., 2018). Nevertheless, the tibia length did not differ to suggest altered developmental growth nor were *Gh*-related transcripts differentially expressed in the hypothalamic transcriptome. Thus, confirmation of both altered pulsatile GH release and regulation would be propitious.

Our analysis revealed further mechanistic insights into the DIO-susceptibility associated with GPR101 loss. Under both dietary conditions, the mutant transcriptomic profile indicated altered hypothalamic inflammatory signalling, microglia, endothelial cell and lipid metabolism-related gene activation. Disrupted TTP activity with GPR101 ablation on CD can produce a chronic inflammatory state seen also in inflammatory arthritis (Ross et al., 2017). This finding of apparent impaired inflammation resolution tallies with the established GPR101 pro-resolving function as the SPM RvD5n-3 receptor (Flak et al., 2020). In addition, obstructed TTP associates with activated microglia, a possibility supported by
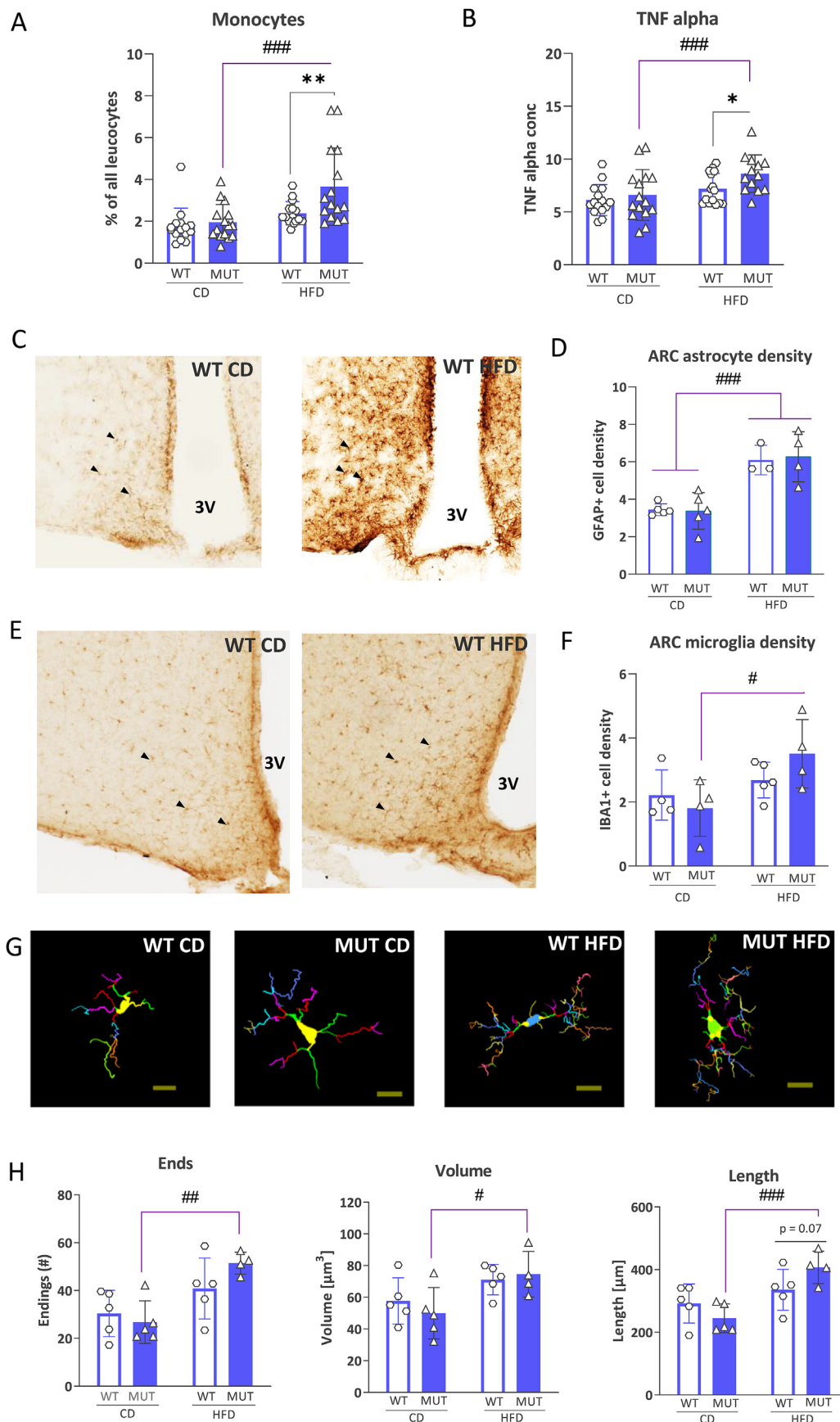
Fig. 4. GPR101 loss altered innate immune response markers and hypothalamic microglial morphology with high-fat diet (HFD) feeding. (A) Graph shows circulating monocytes in HFD-fed *Gpr101* knockout (KO or "MUT") mice compared to both HFD-fed wildtype ("WT" and chow diet (CD)-fed MUT. Circulating tumor necrosis factor (TNF)-alpha, the proinflammatory cytokine, produced by monocytes/macrophages levels measured (B). (C) Representative photomicrographs of the astrocyte marker, glial fibrillary acidic protein (GFAP), immune-staining patterns in WT CD and HFD fed mice. (D) The cell density estimates of GFAP + astrocyte cells with HFD consumption in the hypothalamic arcuate nucleus (ARC) (E) Representative photomicrographs of the Ionized calcium binding adaptor molecule 1 (IBA1)+ microglial marker immunostaining from WT CD and HFD fed mice. (F) The IBA1+ microglia cell density estimates in the ARC are shown. (G, H) Representative morphological tracing of ARC IBA1+ microglia from mice of each group and microglia volume, number of branch ends and branch length in MUT mice compared to CD-fed MUT mice (n = 5 microglia analysed/mouse, n = 5 mice/group for WT + MUT CD, WT for HFD and n = 4 mice/group for HFD MUT). Data comparisons with 2-way ANOVA with post-hoc LSD test. *p<0.05, **p<0.01 WT vs. MUT, #p<0.05, ##p<0.01, ###p<0.001 CD vs. HFD. 3V = third ventricle. Scale bar = 10 mm. Black arrows highlight immuno-stained cells (astrocytes or microglia).

upregulated *Trem2* in CD-fed *Gpr101* KO mice. TREM2 is a lipid-sensitive marker of DAMs that stimulates phagocytosis (Boche and Gordon 2022). In general, hypothalamic microglia sense and initiate inflammatory and phagocytic reactions to dietary excess before metabolic adaptations; a process obstructed in obesity (Mendes et al., 2018). Even without a dietary challenge, activated microglia, as inferred by the transcriptomic profile of *Gpr101* KO mice already on CD, promote weight gain and immune primed-microglia increase DIO susceptibility (Fernandez-Arjona et al., 2022; Valdearcos et al., 2017). After 15 weeks on HFD, the hypothalamic DEG profile in the mutant mice was one of impaired lipid sensing and metabolism and blunted microglial phagocytosis that may have also elevated the DIO risk and/or are responses to protracted nutritional challenge. Within the hypothalamus, microglia are necessary for lipid detection and debris clearance, the impairment of which contributes to their inflammatory activation and excess lipid accumulation (Folick et al., 2021). Thus, GPR101 loss could have accelerated DIO risk on HFD due to inappropriate microglial lipid sensing.

A new microglia classification was defined recently, the so-called 'lipid droplet accumulating microglia' (LDAM) (Marschallinger et al., 2020). These cells are typified by excessive lipid droplet intake, defective phagocytosis and high reactive oxygen species (ROS) and proinflammatory cytokine levels. TTP (ZFP36) interactome genes were among the top differentially expressed in LDAMs (Marschallinger et al., 2020). GPR101 dysfunction may induce LDAM generation as supported by the aberrant lipid metabolism transcriptomic profile. Moreover, the increased microglial end number, volume and branch length in the HFD-fed mutant group infer LDAM-typical decreased phagocytosis (Kettenmann et al., 2011). As the RvD5 receptor in macrophages, GPR101 increases effero- and phago-cytosis (Flak et al., 2020). Microglia also express SPM receptors and can respond to resolvins in neuro-inflammation resolution (Tiberi and Chiurchiu 2021). GPR101 loss likely then undermined the microglial pro-resolving capacity. The concomitant increased vulnerability to LDAM formation can fuel the HFD-induced inflammation, lipid accumulation, impaired phagocytosis, increased POMC + cell loss and elevated DIO risk. A more in-depth scrutiny of GPR101 deficient microglia will shed more light on associated DIO risk.

4.1. Conclusion

To conclude, we have shown that constitutive GPR101 loss in male mice increases the risk for DIO and insulin resistance that may relate to the loss of hypothalamic satiety neurons and microglial pro-resolving inflammation function of this receptor. There is more investigation needed to identify the GPR101 ligand(s) that produce these pathogenic effects as well as the confirmation of the underlying physiological mechanisms. This ideally will include a more comprehensive chronic analysis of energy expenditure, food intake and brown adipose tissue function associated with GPR101 loss in addition to fasting insulin and glucose measurements with ipGTT as well as microglial morphology during the early phase of HFD-induced body weight gain. Furthermore, a cross-species comparison with zebrafish will confirm whether GPR101 KO alters hypothalamic-pituitary development due to overactive Wnt signalling (Trivellin et al., 2021). Nevertheless, these initial gene ablation phenotypes reinforce the therapeutic promise of this receptor for human obesity patients paving the way for additional research into GPR101.

Author contributions (names must be given as initials)

LG, MI, AB, BR, RG, LB, ASM, AAP, RR, YLC, MK, JCW, HF, VGD, SMH, TZ conceptualised the experiment, developed and executed the methodology, performed the formal analysis with statistics, conducted the research and analysed and interpreted the data, wrote the manuscript, reviewed and edited the manuscript. WW, MHdA, TZ and SMH reviewed and edited the manuscript, supervised and lead the research activity. MHdA and WW acquired the funding necessary to conduct the research.

Additional information (including a competing interests statement)

AB and TZ are employees of Boehringer Ingelheim Pharma GmbH & Co. KG. AB and TZ declare no competing financial interest in this work.

Declaration of competing interest

The authors declare the following financial interests/personal relationships which may be considered as potential competing interests: Martin Hrabe de Angelis reports was provided by German Federal Ministry of Education and Research (Infrafrontier grant 01KX1012).

Acknowledgments

Appendix A. Supplementary data

Supplementary data to this article can be found online at https://doi.org/10.1016/j.nsa.2023.101126.

References

Abboud, D., Daly, A.F., Dupuis, N., Bahri, M.A., Inoue, A., Chevigne, A., Ectors, F., Plenevaux, A., Pirotte, B., Beckers, A., Hanson, J., 2020. GPR101 drives growth hormone hypersecretion and gigantism in mice via constitutive activation of Gs and Gq/11. Nat. Commun. 11, 4752.

Acs, P., Bauer, P.O., Mayer, B., Bera, T., Macallister, R., Mezey, E., Pastan, I., 2015. A novel form of ciliopathy underlies hyperphagia and obesity in Ankrd26 knockout mice. Brain Struct. Funct. 220, 1511–1528.

Akiyama, M., Okada, Y., Kanai, M., Takahashi, A., Momozawa, Y., Ikeda, M., Iwata, N., Ikegawa, S., Hirata, M., Matsuda, K., Iwasaki, M., Yamaji, T., Sawada, N., Hachiya, T., Tanno, K., Shimizu, A., Hozawa, A., Minegishi, N., Tsugane, S., Yamamoto, M., Kubo, M., Kamatani, Y., 2017. Genome-wide association study identifies 112 new loci for body mass index in the Japanese population. Nat. Genet. 49, 1458–1467.

Atagi, Y., Liu, C.C., Painter, M.M., Chen, X.F., Verbeeck, C., Zheng, H., Li, X., Rademakers, R., Kang, S.S., Xu, H., Younkin, S., Das, P., Fryer, J.D., Bu, G., 2015. Apolipoprotein E is a ligand for triggering receptor expressed on myeloid cells 2 (TREM2). J. Biol. Chem. 290, 26043–26050.

Bagnol, D., 2010. Use of gpr101 Receptor in Methods to Identify Modulators of Hypothalamic Proopiomelanocortin (POMC)-derived Biologically Active Peptide Secretion Useful in the Treatment of Pomc-Derived Biologically Active Peptide-Related Disorders. US Patent Office (USPTO), U.S. patent No, pp. 1–80, 2010.

Barazzoni, R., Gortan Cappellari, G., Ragni, M., Nisoli, E., 2018. Insulin resistance in obesity: an overview of fundamental alterations. Eat. Weight Disord. 23, 149–157.

Bates, B., Zhang, L., Nawoschik, S., Kodangattil, S., Tseng, E., Kopsco, D., Kramer, A., Shan, Q., Taylor, N., Johnson, J., Sun, Y., Chen, H.M., Blatcher, M., Paulsen, J.E., Pausch, M.H., 2006. Characterization of Gpr101 expression and G-protein coupling selectivity. Brain Res. 1087, 1–14.

Bera, T.K., Liu, X.F., Yamada, M., Gavrilova, O., Mezey, E., Tessarollo, L., Anver, M., Hahn, Y., Lee, B., Pastan, I., 2008. A model for obesity and gigantism due to disruption of the Ankrd26 gene. Proc. Natl. Acad. Sci. U. S. A 105, 270–275.

Boche, D., Gordon, M.N., 2022. Diversity of transcriptomic microglial phenotypes in aging and Alzheimer's disease. Alzheimers Dement 18, 360–376.

Charles-Messance, H., Mitchelson, K.A.J., De Marco Castro, E., Sheedy, F.J., Roche, H.M., 2020. Regulating metabolic inflammation by nutritional modulation. J. Allergy Clin. Immunol. 146, 706–720.

Chen, E.Y., Tan, C.M., Kou, Y., Duan, Q., Wang, Z., Meirelles, G.V., Clark, N.R., Ma'ayan, A., 2013. Enrichr: interactive and collaborative HTML5 gene list enrichment analysis tool. BMC Bioinf. 14, 128.

De Souza, C.T., Araujo, E.P., Bordin, S., Ashimine, R., Zollner, R.L., Boschero, A.C., Saad, M.J., Velloso, L.A., 2005. Consumption of a fat-rich diet activates a proinflammatory response and induces insulin resistance in the hypothalamus. Endocrinology 146, 4192–4199.

Donath, M.Y., Shoelson, S.E., 2011. Type 2 diabetes as an inflammatory disease. Nat. Rev. Immunol. 11 (2), 98–107.

Fernandez-Arjona, M.D.M., Leon-Rodriguez, A., Grondona, J.M., Lopez-Avalos, M.D., 2022. Long-term priming of hypothalamic microglia is associated with energy balance disturbances under diet-induced obesity. Glia 70, 1734–1761.

Flak, M.B., Koenis, D.S., Sobrino, A., Smith, J., Pistorius, K., Palmas, F., Dalli, J., 2020. GPR101 mediates the pro-resolving actions of RvD5n-3 DPA in arthritis and infections. J. Clin. Invest. 130, 359–373.

Folick, A., Koliwad, S.K., Valdearcos, M., 2021. Microglial lipid biology in the hypothalamic regulation of metabolic homeostasis. Front. Endocrinol. 12, 668396.

Franklin, K.B.J., Paxinos, G., 1997. The Mouse Brain in Stereotaxic Coordinates. Academic Press, San Diego. https://doi.org/10.1111/j.1469-7580.2004.00264.x.

Fuchs, H., Aguilar-Pimentel, J.A., Amarie, O.V., Becker, L., Calzada-Wack, J., Cho, Y.L., Garrett, L., Holter, S.M., Irmler, M., Kistler, M., Kraiger, M., Mayer-Kuckuk, P., Moreth, K., Rathkolb, B., Rozman, J., da Silva Buttkus, P., Treise, I., Zimprich, A., Gampe, K., Hutterer, C., Stoger, C., Leuchtenberger, S., Maier, H., Miller, M., Scheideler, A., Wu, M., Beckers, J., Bekeredjian, R., Brielmeier, M., Busch, D.H., Klingenspor, M., Klopstock, T., Ollert, M., Schmidt-Weber, C., Stoger, T., Wolf, E., Wurst, W., Yildirim, A.O., Zimmer, A., Gailus-Durner, V., Hrabe de Angelis, M., 2018. Understanding gene functions and disease mechanisms: phenotyping pipelines in the German Mouse Clinic. Behav. Brain Res. 352, 187–196.

Fuchs, H., Gailus-Durner, V., Adler, T., Pimentel, J.A., Becker, L., Bolle, I., Brielmeier, M., Calzada-Wack, J., Dalke, C., Ehrhardt, N., Fasnacht, N., Ferwagner, B., Frischmann, U., Hans, W., Holter, S.M., Holzlwimmer, G., Horsch, M., Javaheri, A., Kallnik, M., Kling, E., Lengger, C., Maier, H., Mossbrugger, I., Morth, C., Naton, B., Noth, U., Pasche, B., Prehn, C., Przemeck, G., Puk, O., Racz, I., Rathkolb, B., Rozman, J., Schable, K., Schreiner, R., Schrewe, A., Sina, C., Steinkamp, R., Thiele, F., Willershauser, M., Zeh, R., Adamski, J., Busch, D.H., Beckers, J., Behrendt, H., Daniel, H., Esposito, I., Favor, J., Graw, J., Heldmaier, G., Hofler, H., Ivandic, B., Katus, H., Klingenspor, M., Klopstock, T., Lengeling, A., Mempel, M., Muller, W., Neschen, S., Ollert, M., Quintanilla-Martinez, L., Rosenstiel, P., Schmidt, J., Schreiber, S., Schughart, K., Schulz, H., Wolf, E., Wurst, W., Zimmer, A., Hrabe de Angelis, M., 2009. The German Mouse Clinic: a platform for systemic phenotype analysis of mouse models. Curr. Pharmaceut. Biotechnol. 10, 236–243.

Garrett, L., Chang, Y.J., Niedermeier, K.M., Heermann, T., Enard, W., Fuchs, H., Gailus-Durner, V., Angelis, M.H., Huttner, W.B., Wurst, W., Holter, S.M., 2020. A truncating Aspm allele leads to a complex cognitive phenotype and region-specific reductions in parvalbuminergic neurons. Transl. Psychiatry 10, 66.

Garrett, L., Lie, D.C., Hrabe de Angelis, M., Wurst, W., Holter, S.M., 2012. Voluntary wheel running in mice increases the rate of neurogenesis without affecting anxiety-related behaviour in single tests. BMC Neurosci. 13, 61.

Garrett, L., Ung, M.C., Heermann, T., Niedermeier, K.M., Holter, S., 2018. Analysis of neuropsychiatric disease-related functional neuroanatomical markers in mice. Curr. Protoc. Mol. Biol. 8, 79–128.

Gibbons, A.S., Thomas, E.A., Scarr, E., Dean, B., 2010. Low density lipoprotein receptor-related protein and apolipoprotein E expression is altered in schizophrenia. Front. Psychiatr. 1, 19.

Gregg, E.W., Hora, I., Benoit, S.R., 2019. Resurgence in diabetes-related complications. JAMA 321, 1867–1868.

Heermann, T., Garrett, L., Wurst, W., Fuchs, H., Gailus-Durner, V., Hrabe de Angelis, M., Graw, J., Holter, S.M., 2019. Crybb2 mutations consistently affect schizophrenia endophenotypes in mice. Mol. Neurobiol. 56, 4215–4230.

Holter, S.M., Einicke, J., Sperling, B., Zimprich, A., Garrett, L., Fuchs, H., Gailus-Durner, V., Hrabe de Angelis, M., Wurst, W., 2015. Tests for anxiety-related behavior in mice. Curr. Protoc. Mol. Biol. 5, 291–309.

Jao, J., Ciernia, A.V., 2021. MGEnrichment: a web application for microglia gene list enrichment analysis. PLoS Comput. Biol. 17, e1009160.

Jeong, D.Y., Song, N., Yang, H.R., Tu, T.H., Park, B.S., Kang, H., Park, J.W., Lee, B.J., Yang, S., Kim, J.G., 2021. Deficiency of tristetraprolin triggers hyperthermia through enhancing hypothalamic inflammation. Int. J. Mol. Sci. 22.

Jeong, W., Lee, H., Cho, S., Seo, J., 2019. ApoE4-Induced cholesterol dysregulation and its brain cell type-specific implications in the pathogenesis of alzheimer's disease. Mol. Cell. 42, 739–746.

Kallnik, M., Elvert, R., Ehrhardt, N., Kissling, D., Mahabir, E., Welzl, G., Faus-Kessler, T., de Angelis, M.H., Wurst, W., Schmidt, J., Holter, S.M., 2007. Impact of IVC housing on emotionality and fear learning in male C3HeB/FeJ and C57BL/6J mice. Mamm. Genome 18, 173–186.

Keren-Shaul, H., Spinrad, A., Weiner, A., Matcovitch-Natan, O., Dvir-Szternfeld, R., Ulland, T.K., David, E., Baruch, K., Lara-Astaiso, D., Toth, B., Itzkovitz, S., Colonna, M., Schwartz, M., Amit, I., 2017. A unique microglia type associated with restricting development of alzheimer's disease. Cell 169, 1276–1290 e1217.

Kettenmann, H., Hanisch, U.K., Noda, M., Verkhratsky, A., 2011. Physiology of microglia. Physiol. Rev. 91, 461–553.

Kleinberger, G., Yamanishi, Y., Suarez-Calvet, M., Czirr, E., Lohmann, E., Cuyvers, E., Struyfs, H., Pettkus, N., Wenninger-Weinzierl, A., Mazaheri, F., Tahirovic, S., Lleo, A., Alcolea, D., Fortea, J., Willem, M., Lammich, S., Molinuevo, J.L., Sanchez-Valle, R., Antonell, A., Ramirez, A., Heneka, M.T., Sleegers, K., van der Zee, J., Martin, J.J., Engelborghs, S., Demirtas-Tatlidede, A., Zetterberg, H., Van Broeckhoven, C., Gurvit, H., Wyss-Coray, T., Hardy, J., Colonna, M., Haass, C., 2014. TREM2 mutations implicated in neurodegeneration impair cell surface transport and phagocytosis. Sci. Transl. Med. 6, 243ra286.

Kothari, V., Luo, Y., Tornabene, T., O'Neill, A.M., Greene, M.W., Geetha, T., Babu, J.R., 2017. High fat diet induces brain insulin resistance and cognitive impairment in mice. Biochim. Biophys. Acta, Mol. Basis Dis. 1863, 499–508.

Lee, D.K., Nguyen, T., Lynch, K.R., Cheng, R., Vanti, W.B., Arkhitko, O., Lewis, T., Evans, J.F., George, S.R., O'Dowd, B.F., 2001. Discovery and mapping of ten novel G protein-coupled receptor genes. Gene 275, 83–91.

Lumeng, C.N., Saltiel, A.R., 2011. Inflammatory links between obesity and metabolic disease. J. Clin. Invest. 121, 2111–2117.

Marschallinger, J., Iram, T., Zardeneta, M., Lee, S.E., Lehallier, B., Haney, M.S., Pluvinage, J.V., Mathur, V., Hahn, O., Morgens, D.W., Kim, J., Tevini, J., Felder, T.K.,

Wolinski, H., Bertozzi, C.R., Bassik, M.C., Aigner, L., Wyss-Coray, T., 2020. Lipid-droplet-accumulating microglia represent a dysfunctional and proinflammatory state in the aging brain. Nat. Neurosci. 23, 194–208.

Mendes, N.F., Kim, Y.B., Velloso, L.A., Araujo, E.P., 2018. Hypothalamic microglial activation in obesity: a mini-review. Front. Neurosci. 12, 846.

Morrison, H.W., Filosa, J.A., 2013. A quantitative spatiotemporal analysis of microglia morphology during ischemic stroke and reperfusion. J. Neuroinflammation 10, 4.

Ngo, T., Kufareva, I., Coleman, J., Graham, R.M., Abagyan, R., Smith, N.J., 2016. Identifying ligands at orphan GPCRs: current status using structure-based approaches. Br. J. Pharmacol. 173, 2934–2951.

Nilaweera, K.N., Ozanne, D., Wilson, D., Mercer, J.G., Morgan, P.J., Barrett, P., 2007. G protein-coupled receptor 101 mRNA expression in the mouse brain: altered expression in the posterior hypothalamus and amygdala by energetic challenges. J. Neuroendocrinol. 19, 34–45.

Nilaweera, K.N., Wilson, D., Bell, L., Mercer, J.G., Morgan, P.J., Barrett, P., 2008. G protein-coupled receptor 101 mRNA expression in supraoptic and paraventricular nuclei in rat hypothalamus is altered by pregnancy and lactation. Brain Res. 1193, 76–83.

Paul, E.J., Tossell, K., Ungless, M.A., 2019. Transcriptional profiling aligned with in situ expression image analysis reveals mosaically expressed molecular markers for GABA neuron sub-groups in the ventral tegmental area. Eur. J. Neurosci. 50, 3732–3749.

Rathkolb, B., Fuchs, H., Gailus-Durner, V., Aigner, B., Wolf, E., Hrabe de Angelis, M., 2013a. Blood collection from mice and hematological analyses on mouse blood. Curr. Protoc. Mol. Biol. 3, 101–119.

Rathkolb, B., Hans, W., Prehn, C., Fuchs, H., Gailus-Durner, V., Aigner, B., Adamski, J., Wolf, E., Hrabe de Angelis, M., 2013b. Clinical chemistry and other laboratory tests on mouse plasma or serum. Curr. Protoc. Mol. Biol. 3, 69–100.

Rodd, C., Millette, M., Iacovazzo, D., Stiles, C.E., Barry, S., Evanson, J., Albrecht, S., Caswell, R., Bunce, B., Jose, S., Trouillas, J., Roncaroli, F., Sampson, J., Ellard, S., Korbonits, M., 2016. Somatic GPR101 duplication causing X-linked acrogigantism (XLAG)-Diagnosis and management. J. Clin. Endocrinol. Metab. 101, 1927–1930.

Ross, E.A., Naylor, A.J., O'Neil, J.D., Crowley, T., Ridley, M.L., Crowe, J., Smallie, T., Tang, T.J., Turner, J.D., Norling, L.V., Dominguez, S., Perlman, H., Verrills, N.M., Kollias, G., Vitek, M.P., Filer, A., Buckley, C.D., Dean, J.L., Clark, A.R., 2017. Treatment of inflammatory arthritis via targeting of tristetraprolin, a master regulator of pro-inflammatory gene expression. Ann. Rheum. Dis. 76, 612–619.

Saeedi, P., Petersohn, I., Salpea, P., Malanda, B., Karuranga, S., Unwin, N., Colagiuri, S., Guariguata, L., Motala, A.A., Ogurtsova, K., Shaw, J.E., Bright, D., Williams, R., Committee, I.D.F.D.A., 2019. Global and regional diabetes prevalence estimates for 2019 and projections for 2030 and 2045: results from the international diabetes federation diabetes atlas. Diabetes Res. Clin. Pract. 157, 107843, 9(th) edition.

Saito, T., Kuma, A., Sugiura, Y., Ichimura, Y., Obata, M., Kitamura, H., Okuda, S., Lee, H.C., Ikeda, K., Kanegae, Y., Saito, I., Auwerx, J., Motohashi, H., Suematsu, M., Soga, T., Yokomizo, T., Waguri, S., Mizushima, N., Komatsu, M., 2019. Autophagy regulates lipid metabolism through selective turnover of NCoR1. Nat. Commun. 10, 1567.

Schmitz, C., Hof, P.R., 2005. Design-based stereology in neuroscience. Neuroscience 130 (4), 813–831.

Sharma, R., Luong, Q., Sharma, V.M., Harberson, M., Harper, B., Colborn, A., Berryman, D.E., Jessen, N., Jorgensen, J.O.L., Kopchick, J.J., Puri, V., Lee, K.Y., 2018. Growth hormone controls lipolysis by regulation of FSP27 expression. J. Endocrinol. 239, 289–301.

Steuernagel, L., Lam, B.Y.H., Klemm, P., Dowsett, G.K.C., Bauder, C.A., Tadross, J.A., Hitschfeld, T.S., Del Rio Martin, A., Chen, W., de Solis, A.J., Fenselau, H., Davidsen, P., Cimino, I., Kohnke, S.N., Rimmington, D., Coll, A.P., Beyer, A., Yeo, G.S.H., Bruning, J.C., 2022. HypoMap-a unified single-cell gene expression atlas of the murine hypothalamus. Nat Metab 4, 1402–1419.

Szklarczyk, D., Gable, A.L., Lyon, D., Junge, A., Wyder, S., Huerta-Cepas, J., Simonovic, M., Doncheva, N.T., Morris, J.H., Bork, P., Jensen, L.J., Mering, C.V., 2019. STRING v11: protein-protein association networks with increased coverage, supporting functional discovery in genome-wide experimental datasets. Nucleic Acids Res. 47, D607–D613.

Tiberi, M., Chiurchiu, V., 2021. Specialized pro-resolving lipid mediators and glial cells: emerging candidates for brain homeostasis and repair. Front. Cell. Neurosci. 15, 673549.

Trivellin, G., Tirosh, A., Hernández-Ramírez, L.C., Gupta, T., Tsai-Morris, C.H., Faucz, F.R., Burgess, H.A., Feldman, B., Stratakis, C.A., 2021. The X-linked acrogigantism-associated gene gpr101 is a regulator of early embryonic development and growth in zebrafish. Mol. Cell. Endocrinol. 520, 111091.

Trivellin, G., Bjelobaba, I., Daly, A.F., Larco, D.O., Palmeira, L., Faucz, F.R., Thiry, A., Leal, L.F., Rostomyan, L., Quezado, M., Schernthaner-Reiter, M.H., Janjic, M.M., Villa, C., Wu, T.J., Stojilkovic, S.S., Beckers, A., Feldman, B., Stratakis, C.A., 2016. Characterization of GPR101 transcript structure and expression patterns. J. Mol. Endocrinol. 57, 97–111.

Trivellin, G., Daly, A.F., Faucz, F.R., Yuan, B., Rostomyan, L., Larco, D.O., Schernthaner-Reiter, M.H., Szarek, E., Leal, L.F., Caberg, J.H., Castermans, E., Villa, C., Dimopoulos, A., Chittiboina, P., Xekouki, P., Shah, N., Metzger, D., Lysy, P.A., Ferrante, E., Strebkova, N., Mazerkina, N., Zatelli, M.C., Lodish, M., Horvath, A., de Alexandre, R.B., Manning, A.D., Levy, I., Keil, M.F., Sierra Mde, L., Palmeira, L., Coppieters, W., Georges, M., Naves, L.A., Jamar, M., Bours, V., Wu, T.J., Choong, C.S., Bertherat, J., Chanson, P., Kamenicky, P., Farrell, W.E., Barlier, A., Quezado, M., Bjelobaba, I., Stojilkovic, S.S., Wess, J., Costanzi, S., Liu, P., Lupski, J.R., Beckers, A., Stratakis, C.A., 2014. Gigantism and acromegaly due to Xq26 microduplications and GPR101 mutation. N. Engl. J. Med. 371, 2363–2374.

Trotta, M., Bello, E.P., Alsina, R., Tavella, M.B., Ferran, J.L., Rubinstein, M., Bumaschny, V.F., 2020. Hypothalamic Pomc expression restricted to GABAergic

neurons suppresses Npy overexpression and restores food intake in obese mice. Mol. Metabol. 37, 100985.

Ulrich, J.D., Holtzman, D.M., 2016. TREM2 function in alzheimer's disease and neurodegeneration. ACS Chem. Neurosci. 7, 420–427.

Ung, M.C., Garrett, L., Dalke, C., Leitner, V., Dragosa, D., Hladik, D., Neff, F., Wagner, F., Zitzelsberger, H., Miller, G., de Angelis, M.H., Rossler, U., Vogt Weisenhorn, D., Wurst, W., Graw, J., Holter, S.M., 2021. Dose-dependent long-term effects of a single radiation event on behaviour and glial cells. Int. J. Radiat. Biol. 97, 156–169.

Valdearcos, M., Douglass, J.D., Robblee, M.M., Dorfman, M.D., Stifler, D.R., Bennett, M.L., Gerritse, I., Fasnacht, R., Barres, B.A., Thaler, J.P., Koliwad, S.K., 2017. Microglial inflammatory signaling orchestrates the hypothalamic immune response to dietary excess and mediates obesity susceptibility. Cell Metabol. 26, 185–197 e183.

Valdearcos, M., Robblee, M.M., Benjamin, D.I., Nomura, D.K., Xu, A.W., Koliwad, S.K., 2014. Microglia dictate the impact of saturated fat consumption on hypothalamic inflammation and neuronal function. Cell Rep. 9, 2124–2138.

Wacker, D., Stevens, R.C., Roth, B.L., 2017. How ligands illuminate GPCR molecular pharmacology. Cell 170, 414–427.